Sequential electron emission and nuclear dissociation after the O $1s \rightarrow (^4\Sigma_u^-)4p\sigma$ excitation in O₂ molecules

Shan Song,[1,2] Bocheng Ding,[2] Weiqing Xu,[2] Christophe Nicolas,[3] Minna Patanen,[3,4] Saikat Nandi,[3] John Bozek,[3] Catalin Miron,[5,6] Zhisong Xiao,[1] and Xiao-Jing Liu[1,2,*]

[1]*School of Physics and Nuclear Energy Engineer, Beihang University, Xueyuan Road, Beijing 100191, China*
[2]*School Physical Science and Technology, ShanghaiTech University, Shanghai 201210, China*
[3]*Synchrotron SOLEIL, l'Orme des Merisiers, Saint-Aubin, BP 48, 91192 Gif-sur-Yvette Cedex, France*
[4]*Nano and Molecular Systems Research Unit, Molecular Materials Research Community, Faculty of Science, University of Oulu, P.O. Box 3000, 90014 Oulu, Finland*
[5]*LIDYL, CEA, CNRS, Université Paris-Saclay, CEA Saclay, 91191 Gif-sur-Yvette, France*
[6]*Extreme Light Infrastructure Nuclear Physics (ELI-NP), "Horia Hulubei" National Institute for Physics and Nuclear Engineering, 30 Reactorului Street, RO-077125 Măgurele, Jud. Ilfov, Romania*

When an electron is resonantly excited from a core orbital to a Rydberg one in a molecule, complex multi-time-scale multistep processes are triggered. By using a high-resolution energy-resolved coincidence between Auger electron and ions, we identified the sequences of processes following the spectator Auger decays induced by K-shell excitation in O₂. The first step of the spectator Auger decay can end up to a few metastable O_2^+ states which autoionize into stable O_2^{2+}. However, the majority of O_2^+ states are dissociative. They evolve into several dissociation limits with complex crossings between potential-energy curves. After the molecular dissociation is finished, the generated fragments can further decay either by fluorescence emission or by autoionization. Interestingly, some electrons are always emitted after molecular dissociation.

I. INTRODUCTION

The absorption of a soft x-ray photon can promote an electron from a core orbital to a valence or Rydberg one, triggering relaxation processes such as soft x-ray photon emission, resonant Auger electron emission, deformation of molecular structure, secondary Auger electron emission, etc. As one of the simplest open-shell molecules, O₂ constitutes a testbed of these decay processes. The photoabsorption spectrum of O₂ molecule below the O $1s\sigma^{-1}$ ionization threshold has been a subject to many experimental and theoretical investigations over an extended period (e.g., Refs. [1–7]). Although the O $1s\sigma^{-1} \rightarrow 1\pi_g^*$ resonances present a relatively simple vibrational structure [8], the σ^* resonances and Rydberg series present a much richer structure due to the overlap between the broad σ^* resonances and discrete states converging to the $1s^{-1}\,^4\Sigma_u^-$ and $1s^{-1}\,^2\Sigma_u^-$ ionization thresholds at 543.39 and 544.43 eV [9], respectively.

Resonant Auger electron spectroscopy is a powerful tool to study electronic structure in the inner-valence spectral region [10–14]. After a core electron excitation, the molecule mainly decays by emitting one electron, while the excited electron may participate in Auger decay or standby like a spectator. Tanaka *et al.* [15] comprehensively measured the high-resolution absorption spectrum and a series of resonant spectator Auger-electron spectra of O₂. They assigned many of the observed spectator Auger final states in terms of

cationic Rydberg series by using a spectator-electron shake relaxation model.

The dissociative character of the excited intermediate state and the Auger final states is the source of very rich dynamics, where the electronic relaxation and the nuclear motion can occur on the same time scale. Indeed, the molecular dissociation in the intermediate state can be even faster than the resonant Auger decay [13,16–18] (see [19] for a review of the phenomenon). Dicationic O_2^{2+} from normal Auger decays and the cationic O_2^+ from participator-Auger decay can also be reached other ionization methods. Using Doppler-free kinetic release spectroscopy and multireference configuration-interaction calculations, the potential-energy curves of O_2^{2+} were reported by Lundqvist *et al.* [20]. Using threshold photoelectron-photoion coincidence, Hikosaka *et al.* [21] found that most of the inner-valence-hole states of O_2^+ are strongly dissociative. Using electron-electron coincidence incorporated in a magnetic bottle spectrometer [22], Feifel *et al.* [23] demonstrated that, near the double-ionization threshold of O₂, a dissociative ionization path is likely to be followed by autoionization of an oxygen atom.

By measuring the electron kinetic energy coincide with the ion time of flight (TOF), partial electron spectra relevant to different ionic species are obtained [24], and the decay-dissociation dynamics can be inferred from the profile of peaks in the TOF spectrum [24,25]. With both electron momenta and ion momenta fully measured, the COLd-Target-Recoil-Ion-Momentum-Spectrometer (COLTRIMS) or Reaction-microscope [26,27] is extremely successful in a coincident experiment with low electron kinetic energy.

*liuxj@shanghaitech.edu.cn

Combining COLTRIMS with an ultrafast laser, the occurrence of atomic autoionization in O_2 was traced by Sandhu *et al.* [28]. With a deceleration voltage added to the electron arm, COLTRIMS can also be used to measure high-energy electron [29]; the price paid is that the electron collection efficiency is reduced to about 1%. With Èlectron-PhotoIon-Coïncidence-en-Ènergie-Appareil (EPICEA) some of us pointed out an analogy between the resonant Auger electron emission from an ultrafast dissociative O_2 molecule and the recoiling Young's double slit experiment [17].

In this work, we measured the correlation between the spectator-Auger electrons and ionic fragments after O $1s\sigma \rightarrow (1s^{-1}\,^4\Sigma_u^-)4p\sigma/(1s^{-1}\,^2\Sigma_u^-)3p'\sigma$ excitation in O_2 at the photon energy of 541.8 eV. A few nondissociative Auger final states were identified. From the correlation between the electron kinetic energy and the ion kinetic energy, we were able to distinguish different dissociation pathways. The results highlight how the spectator Rydberg electron participates in the dissociation of the Auger final states.

II. EXPERIMENTAL METHOD

The experiments were carried out using the EPICEA setup at the PLEIADES beamline [30,31] at synchrotron SOLEIL in Saint-Aubin, France. This setup is specially designed for high kinetic-energy electron-ion coincidence measurement, i.e., to study the electron emission in the molecular frame after inner-shell excitation or ionization. This setup is composed of a double-toroidal electron analyzer (DTA) [32–34] and an ion TOF spectrometer. Electron spectra were recorded using the DTA fitted with a gas needle, which is placed between two flat grids (pusher and extractor for ion). The energy-dispersed electrons passing through the analyzer are recorded by a DLD40 delay-line detector from Roentdek Handels GmbH [35]. Auger electrons are collected at the magic angle, i.e., with an emission direction in the polar angle of $54 \pm 3°$ with respect to the symmetry axis of DTA and the azimuthal angles from $0°$ to $360°$, which corresponds to a collection angle of 0.53 steradian (4% of full 4π). This high acceptance angle makes the DTA very attractive for coincidence experiments. The detection efficiency for an electron is about 60%. The energy resolution is around 0.8% of the pass energy. In the present work, the photon energy is selected at 541.8 eV with vertical polarization, parallel to the symmetry axis of the DTA (see [31]). DTA is operated with the pass energy of 80 eV, the central kinetic energy of 503 eV, and the electron energy resolution of 0.7 eV.

Opposite to the electron side, there is an ion TOF spectrometer incorporating 3D focusing. A pulsed ± 100 V voltage triggered by the electron signal is applied to the pusher and extractor of the TOF spectrometer, pushing the ionic fragments to the ion detector. Ions with the kinetic energies below 10 eV are fully collected on the detector, while the detection efficiency of an ion is about 35%. The mass resolution of the nearly zero kinetic-energy ions is about 1000, the ion momentum resolution is about 1.2–1.6 a.u, and the ion energy resolution is about 0.3 eV. Since the ion collection is triggered by the detection of an electron and experiment was done at multibunch mode (2.8 ns between nearby two bunched), many ions created by the previous events might stay near the
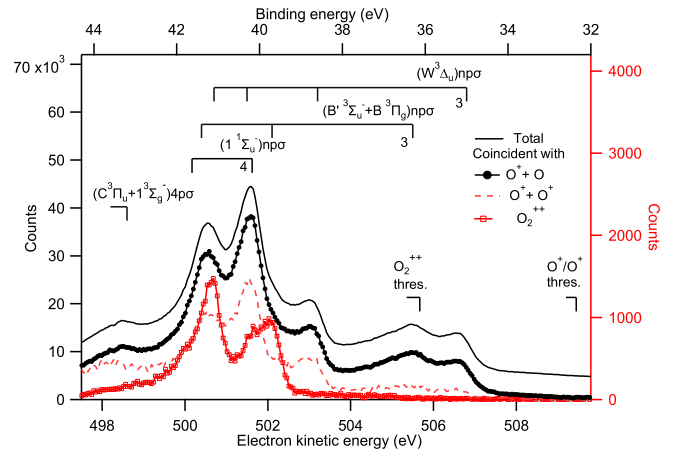
FIG. 1. Resonant Auger electron spectrum (rAES) recorded at 541.8 eV photon energy. The total Auger electron spectrum and the partial Auger electron spectra recorded in coincidence with different ionic combinations are illustrated with different colors and symbols. The total rAES is shifted upward for clarity. The curves corresponding to $O^+ + O^+$ and O_2^{2+} are plotted to apply to the right axis due to their very low intensity. Except for the long-lived $(1\,^1\Sigma_u^-)(4, 5)p\sigma$ states, all the other assignments are adopted from Tanaka *et al.* [15].

interaction region, which results in the false coincidence. A random signal generator is used to trigger the pulsed high voltage and thus push the ions randomly to the detector so that the false events are constructed. The count rate of electrons is kept at $100\ s^{-1}$, the same as the repetition rate of the random signal. The contribution from the false coincidence is removed according to the method described by Prümper *et al.* [36].

III. RESULT AND DISCUSSION

The total resonant Auger electron energy spectrum (rAES) recorded at a photon energy of 541.8 eV is shown in Fig. 1, which covers the kinetic-energy range from 497.5 to 509 eV (corresponding to a binding energy range from 32.8 to 44.3 eV). Our spectrum with an energy resolution of 0.7 eV agrees reasonably with the high resolution one of Tanaka *et al.* [15]. The two lowest Rydberg series, $(X\,^1\Sigma_g^+)np\sigma$ and $(A\,^3\Sigma_u^+)np\sigma$, cannot be reached by resonant Auger decay due to the selection rules. The assignments, except for the $(1\,^1\Sigma_u^-)4, 5p\sigma$ states, are adopted from Tanaka [15] as cationic Rydberg series.

The ion TOF spectra of all ions before and after random coincidence subtraction are shown in Fig. 2. The contribution of random coincidence is about 30% for O^+ and O_2^{2+}. Because the measurement is quite time consuming (about 10 h for one data set at one selected photon energy and binding energy region), this ratio of 30% is a good compromise between the good statistics and low random contribution [36]. While the peaks of O^{2+} and O_2^+ can be seen in the original TOF spectrum before the subtraction of random coincidence, they almost completely disappear in the true TOF spectrum after the subtraction of random coincidence. This phenomenon is due to two reasons. First, it is impossible to produce O^{2+} within the range of the measured electron binding energy.
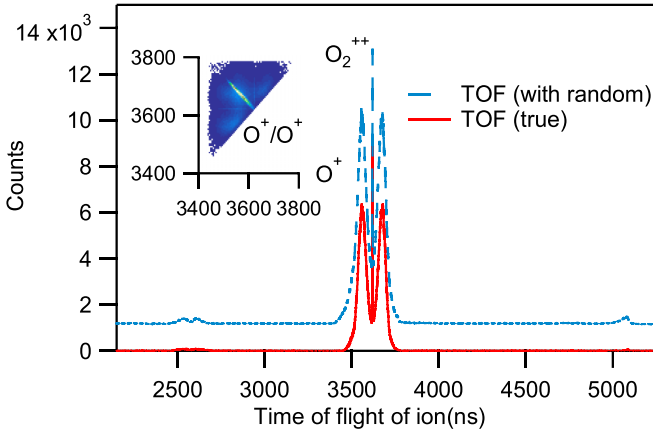
FIG. 2. TOF spectra of all ions before (dashed blue line) and after (solid red line) the random coincidence is removed, where the TOF spectrum with random is shifted up for clarity. The photoion-photoion coincidence map is plotted as an inset.

Second, the states that are stable against dissociation and autoionization are $(X \, ^1\Sigma_g^+)np\sigma$, but they cannot be reached due to the selection rules. In the true TOF spectrum, O^+ and O_2^{2+} represent 98.2% and 1.7% of the count of all ions, respectively. The O_2^{2+} peak stands out sharply due to the nearly zero kinetic energy of the doubly charged parent ions. In contrast to O_2^{2+}, the profile of O^+ is very broad and split into two wings, because $1s\sigma \rightarrow 4p\sigma$ excitation occurs preferentially when the molecular axis is parallel to the polarization vector of the incoming photons (the axis of TOF spectrometer in the present case), and the molecular orientation is preserved during molecular fragmentation, which is generally faster than molecular rotation in this case. The production of O_2^+ is extremely weak, about three times weaker than random coincidence, thus being seriously contaminated so that we were unable to make any meaningful discussion for it. Part of O^+ comes from fragmentation of unstable O_2^{2+}. Due to momentum conservation, these O^+/O^+ pairs are plotted as a diagonal line with a slope of -1 in photoion-photoion-coincidence map, as shown by the inset in Fig. 2. The number of O^+/O^+ pairs amounts to 2.6% of all ions. Taking into account an ion detection efficiency of 35%, about $2.6\%/0.35 \times 2 = 15\%$ of ions come from O^+/O^+ pairs, where the number of O^+/O^+ is 7.5% of that of all ions. We concluded that most Auger final states undergo dissociation, autoionization, or both. The possible decay processes are summarized as

$$O_2\left(1s\sigma^{-1}\,^4\Sigma_u^-\right)4p\sigma \rightarrow O_2^+ + e_{\text{Auger}}^-, \tag{1}$$

$$\rightarrow \begin{cases} O^+ + O, & (2) \\ O^+ + O^+ + e_{\text{auto}}^-, & (3) \\ O_2^{2+} + e_{\text{auto}}^-, & (4) \end{cases}$$
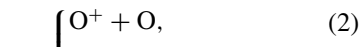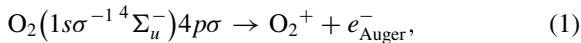
where processes (2), (3), and (4) represent $(98.2 - 15)/(100 - 7.5)\% = 90\%$, $7.5/(100 - 7.5)\% = 8.1\%$, and $1.7/(100 - 7.5)\% = 1.8\%$ of all events, respectively.

To show the relationship between the dissociation and the Auger electron emission, we plotted partial rAESs associated with the reaction processes (2), (3), and (4) in Fig. 1, where the total rAES is shifted upward for clarity. The partial rAES

coincident with $(O^+ + O)$ is almost identical to the total rAES. In the partial rAES coincident with $(O^+ + O^+)$, we could find all the features in the rAES coincident with $(O^+ + O)$, since their binding energy is above the appearance threshold of $(O^+ + O^+)$ by at least 2 eV. Moreover, it can be seen that the ratio $N(O^+ + O^+)/N(O^+ + O)$ increases monotonically as the binding energy increases, which suggests that the fragment O atom would be more likely to autoionize as more energy resides in the resonant Auger final state.

The partial rAES coincident with O_2^{2+} is dramatically different from the other ones. The two peaks with the lowest binding energies are absent. The peak of $(W \, ^3\Delta_u)3p\sigma$ is absent because its binding energy is below the appearance threshold of O_2^{2+} of 36.13 eV [37]. The absence of the peak of $(B' \, ^3\Sigma_u^- + B \, ^3\Pi_g)3p\sigma$ can be understood considering the following aspects: first, its binding energy is only 0.17 eV above the appearance threshold of O_2^{2+}; second, we assume that near the equilibrium internuclear distance the potential-energy curve of a two-hole-one-Rydberg-electron state is similar to that of the corresponding two-hole state, and that they start to deviate from each other at internuclear distances close to or higher than the radius of the Rydberg orbital, allowing us to use the potential-energy curves of O_2^{2+} for the discussion; third, the equilibrium internuclear distances of the $X \, ^1\Sigma_g^+$, $B \, ^3\Pi_g$, and $B' \, ^3\Sigma_u^-$ states of O_2^{2+} are 1.05, 1.21, and 1.35 Å [20], respectively. As a result, the excess energy of 0.17 eV does not allow the autoionization of $O_2^+[(B' \, ^3\Sigma_u^- + B \, ^3\Pi_g)3p\sigma] \rightarrow O_2^{2+}[X \, ^1\Sigma_g^+] + e_{\text{auto}}^-$ to happen vertically without a change of the internuclear distance. For the peaks with higher binding energies, as discussed in our recent paper [38], the dissociation lifetimes of the dicationic $W \, ^3\Delta_u$ and $B \, ^3\Pi$ states are shorter than 0.7 ns and 3.5 ns, respectively, but the dissociation lifetime of $B' \, ^3\Sigma_u^-(v = 0)$ can be as long as several μs [20,39]. Since the effective quantum number n^* of Rydberg states ($n > 4$) is larger than 3.56 [15], the radius of the Rydberg electron is larger than 3.36 Å. This radius is outside both the tunneling barrier and the crossing point of the potential-energy curves of O_2^{2+}, so that the dissociation of the two-hole-one-Rydberg-electron states can be assumed to be similar to those of corresponding dicationic state when the internuclear distance is shorter than 3.36 Å. Also the states $C \, ^3\Pi_u$ and $1 \, ^3\Sigma_g^+$ of O_2^{2+} are strongly dissociative. So, only the $B' \, ^3\Sigma_u^-(v = 0)np\sigma$ ($n = 4, 5$) states are metastable against dissociation and autoionize into O_2^{2+} in the ground state. Moreover, there is another peak at 0.5 eV binding energy higher than the $B' \, ^3\Sigma_u^-(v = 0)np\sigma$ ($n = 4$) state. This peak might be assigned to $(W \, ^3\Delta_u)5p\sigma$ at the first sight, which is however dissociative. Or, we noticed that, in the potential-energy curves of O_2^{2+} by Lundqvist [20], the binding energy of the $1 \, ^1\Sigma_u^-$ is 0.5 eV above that of the $B \, ^3\Sigma_u^-$. In addition, Edvardsson predicted that the dissociation lifetimes of $1 \, ^1\Sigma_u^-(v = 0, 1)$ are 5.12 ms and 10.44 μs, respectively [39]. So we assigned this peak to the $(1 \, ^1\Sigma_u^-)4p\sigma$ state. There is also a weak but visible shoulder at 0.5 eV binding energy higher than the $[B \, ^3\Sigma_u^-(v = 0)]np\sigma$ ($n = 5$) state, which is assigned to the $(1 \, ^1\Sigma_u^-)5p\sigma$ state. The lowest member of this Rydberg series, the $(1 \, ^1\Sigma_u^-)3p\sigma$ state, is absent because, with its binding energy only 0.7 eV above the O_2^{2+} formation threshold, O_2^{2+} can't be produced by
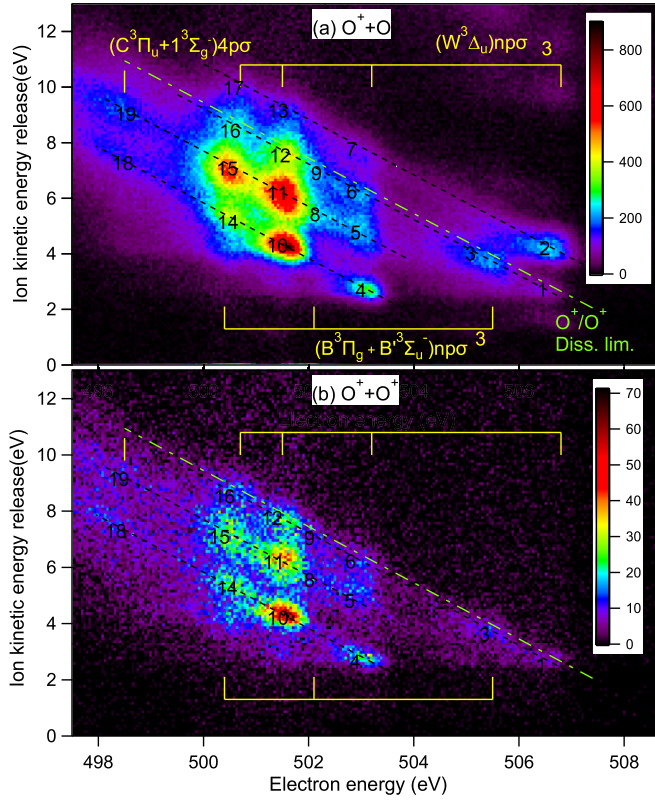
FIG. 3. Correlation between the kinetic energy of spectator Auger electron and the kinetic-energy release of the fragments, where the final fragments are (a) $O^+ + O$ and (b) $O^+ + O^+$, respectively. The diagonal dashed lines correspond to different groups of dissociation limits after spectator Auger decay. The dashed-dotted line indicates the appearance threshold of $O^+ + O^+$.

vertical autoionization. It should be noted that the Auger decay to $(1\,^1\Sigma_u^-)np\sigma$ is usually neglected in the discussion of the resonant Auger spectrum because the ground state of O_2 is $X\,^3\Sigma_g^-$. Here, by measuring the electrons in coincidence with O_2^{2+}, its contribution emerges due to its long lifetime against dissociation.

To further explore the dissociation dynamics of the Auger final states, we plotted the kinetic-energy release of the fragments (the sum of the kinetic energies of all fragments) against the electron kinetic energy for the processes (2) and (3) in Figs. 3(a) and 3(b), respectively. For process (2), the kinetic energy of the neutral atom is assumed to be the same as that of the ion, and the electron recoil momentum needs to be taken into account. For process (3) where both ions are measured, the momentum conservation law is used to correct for the spectral broadening related to the thermal motion so that the resolution of kinetic-energy release gets improved in Fig. 3(b). By comparing Figs. 3(a) and 3(b), we could see that, except for the features above the line that represent the appearance threshold of O^+/O^+, all features in Fig. 3(a) find their counterpart in Fig. 3(b) at the same position and the relative intensities among various features are almost the same. This observation is puzzling due to two reasons. First, the kinetic-energy release for the O^+/O^+ pair is normally expected to be higher than that for the O^+/O due to the

more repulsive Coulombic potential. Second, the reaction probabilities normally depend on the specific fragment.

To facilitate the discussion, the features in Fig. 3(a) are labeled with numbers ranging from 1 to 19. Features 1 to 17 result from the dissociation of the Auger final states $(W\,^3\Delta_u)np\sigma$, $(B\,^3\Pi_g)np\sigma$, and $(B'\,^3\Sigma_u^-)np\sigma$, while features 18 and 19 result from the dissociation of the Auger final state $(C\,^3\Pi_u + 1\,^3\Sigma_g^-)4p\sigma$. The same labels are also used to label the features in Fig. 3(b). While there is one valley between features 4 and 10, and another one between features 7 and 13, respectively, the valleys between features 5 and 11 and between features 6 and 12 are filled. In addition, the features 4, 5, 6, and 7 result from $(W\,^3\Delta_u)4p\sigma$, and the features 10, 11, 12, and 13 result from $(W\,^3\Delta_u)5p\sigma$. So the intensity between features 5 and 11 is assigned as feature 8, and that between features 6 and 12 is assigned as feature 9, respectively. Features 8 and 9 are contributed by $(B\,^3\Pi_g + B'\,^3\Sigma_u^-)4p\sigma$. Although for $(W\,^3\Delta_u)4p\sigma$ the intensity $I_4 > I_5 > I_6 > I_7$, and for $(W\,^3\Delta_u)5p\sigma$ $I_{10} > I_{11} > I_{12} > I_{13}$, but $I_{15} > I_{14} > I_{16} > I_{17}$. This is because I_{15} and I_{16} contain the contribution from both $(W\,^3\Delta_u)6p\sigma$ and $(B\,^3\Pi_g + B'\,^3\Sigma_u^-)5p\sigma$, but I_{14} and I_{17} contain only the contribution from $(W\,^3\Delta_u)6p\sigma$.

These features can be connected by diagonal lines with the slope of -1 due to the energy-conservation law in reaction (2):

$$E(h\nu) = E_k(e_{Auger}^-) + E_{KER} + E_i(O)$$
$$+ E_i(O^+) + E_{IP}(O) + E_D(O_2). \quad (5)$$

Here $E(h\nu)$ is the photon energy, $E_k(e_{Auger}^-)$ is the kinetic energy of the resonant Auger electron, E_{KER} is the kinetic-energy release of fragments in the dissociation processes, $E_i(O)$ and $E_i(O^+)$ are the excitation energies of the atom and ion, respectively, $E_{IP}(O)$ is the ionization potential of the oxygen atom, and $E_D(O_2)$ is the dissociation energy of O_2 molecule at the ground state. The dissociation limit energy E_{diss} is defined as

$$E_{diss} = E_i(O) + E_i(O^+) + E_{IP}(O) + E_D(O_2) \quad (6)$$
$$= E(h\nu) - E_k(e_{Auger}^-) - E_{KER}. \quad (7)$$

The higher the offset of the diagonal line is, the lower E_{diss} is.

Using Eq. (6) and the energy values from the NIST atomic database [40], we calculated for various fragment combinations the possible E_{diss}, which should fall into the ranges defined by Eq. (7) in Fig. 3(a). Since the electronic configurations of $W\,^3\Delta_u$, $B\,^3\Pi_g$, and $B'\,^3\Sigma_u^-$ are dominated by $1\pi_u^{-1}1\pi_g^{-1}$, $3\sigma_g^{-1}1\pi_g^{-1}$, and $1\pi_u^{-1}1\pi_g^{-1}$, respectively, the fragment states with $2\,s^{-1}$ hole are neglected. The Rydberg states with very high principal quantum number ($n > 9$) are not included in the table because they are completely overlapped at our energy resolution. With a full width from 1 to 1.4 eV, each diagonal line represents a group of E_{diss}; the assignments of the fragments are summarized in Table I. With the lifetimes of LS-allowed autoionization states around 1 ps [41], an excited O atom can survive until most of the molecular dissociation processes are completely finished. When the energy of an excited oxygen atom O* lies above the first ionization threshold, an electron can be emitted due to atomic autoionization with low kinetic energy E_{auto}. The

TABLE I. Assignments of the dissociation limits E_{diss} of the spectator Auger final states of O$_2$. Autoionization can occur if the energy of the O atom is above its ionization threshold. The unit of energy is eV.

| O* | E_{auto} | $(O^+)^4S$ | | $(O^+)^2D$ | | $(O^+)^2P$ | |
		E_{diss}	Label	E_{diss}	Label	E_{diss}	Label
$(^4S)3s$		28		31.32	2,7,13,17	33.02	1,3,6,9,12,16
$(^4S)3p$		29.55		32.87	1,3,6,9,12,16	34.57	5,8,11,15
$(^4S)4s, 3d$		30.65	2,7,13,17	33.97	5,8,11,15	35.67	4,10,14
$(^4S)4p$		31	2,7,13,17	34.32	5,8,11,15	36.02	4,10,14
$(^2D)3s$		31.3	2,7,13,17	34.62	5,8,11,15	36.32	4,10,14
$(^4S)5s, 4d, 4f, 5p$		31.45	2,7,13,17	34.77	5,8,11,15	36.47	4,10,14
$(^4S)6s, 5d$		31.75	2,7,13,17	35.07	5,8,11,15		
$(^4S)7s, 6d, 6f, 6g$		31.94	1,3,6,9,12,16	35.26	5,8,11,15		
$(^4S)8s, 7d, 7f$		32.04	1,3,6,9,12,16	35.36	4,10,14		
$(^2D)3p$	0.48	32.8	1,3,6,9,12,16	36.12	4,10,14		
$(^2P)3s$	0.58	32.9	1,3,6,9,12,16	36.22	4,10,14		
$(^2D)4s, 3d, 4p$	1.8	33.9	5,8,11,15				
$(^2P)3p$	2.18	34.5	5,8,11,15				
$(^2D)5s, 4d, 4f$	2.43	34.75	5,8,11,15				
$(^2D)6s, 5d$	2.73	35.05	5,8,11,15				
$(^2D)8s, 7d, 9s, 8d$	3.08	35.4	4,10,14				
$(^2P)4s, 3d$	3.35	35.55	4,10,14				

autoionization lines at kinetic energy from 0.4 to 3.1 eV (see Table I) were observed in independently measured electron energy spectra [42,43].

Rather complex dissociation paths of the spectator Auger final states are observed in Fig. 3 and Table I. For example, the dissociation of the dicationic state O$_2^{2+}$(W $^3\Delta_u$) was described by Lundqvist *et al.* by taking into account the spin-orbit coupling between different electronic states [20]:

$$\mathrm{O}_2^{2+}(\mathrm{W}\,^3\Delta_u) \rightarrow \mathrm{O}^+(^4S) + \mathrm{O}^+(^2D).$$

Here, by additionally involving a $3p\sigma$ Rydberg electron, the dissociation becomes more complicated:

$$\mathrm{O}_2^+(\mathrm{W}\,^3\Delta_u)3p\sigma \rightarrow \mathrm{O}^+(^4S) + \mathrm{O}(^4S)(4s, 3d, 4p, \dots),$$
$$\mathrm{or}\ \mathrm{O}^+(^4S) + \mathrm{O}(^2D)3s,$$
$$\mathrm{or}\ \mathrm{O}^+(^2D) + \mathrm{O}(^4S)3s.$$
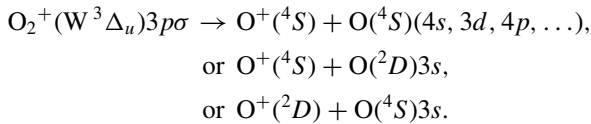
Because energy and spin are exchanged between Rydberg electron and valence electrons during dissociation, when an $np\sigma(n > 4)$ Rydberg electron is included, almost all dissociation limits can be reached.

Because of the very large amount of channels involved, it is very difficult to calculate the full potential-energy curves of the two-hole-one-electron Auger final states and track down their dissociation products theoretically, so far not available in the literature. The assignments in Table I tell us that the spectator Rydberg electron resides on the neutral atom even after the dissociation is finished. The Rydberg electron will face the change of the Coulombic potential as the charge changes approximately from 2 to 1 during the molecular dissociation. The energy will be inevitably exchanged between the Rydberg electron and the ionic core during the molecular dissociation. It is expected that a spectator-Auger final state with an excited Rydberg electron would pass a lot of potential curve cross points before dissociation is accomplished. The quantum system can either stay on the original potential-energy curve or switch to another one at each crossing point and finally evolve into a lot of dissociation limits, as indicated in Fig. 3 and Table I.

IV. SUMMARY

By using the energy-resolved Auger electron-ion coincidence technique, we investigated the molecular fragmentation and the secondary electronic decay channels following spectator Auger decays after an O 1s core electron is resonantly excited to the $4p\sigma$ orbital in O$_2$ molecule. We found that O$_2^{2+}$ is selectively produced by autoionization of the $[\mathrm{B}'\,^3\Sigma_u^-(\nu = 0)]np\sigma$ $(n = 4, 5)$ and $(1\,^1\Sigma_u^-)np$, σ $(n = 4, 5)$ states. Although $(1\,^1\Sigma_u^-)np\sigma$ series is very weak due to propensity rules, it is clearly observed here due to the efficient detection of O$_2^{2+}$ produced by the autoionization of $(1\,^1\Sigma_u^-)np\sigma$ states before they have time to dissociate. Most spectator Auger final states dissociate into O$^+$/O*. O* can decay either by fluorescence emission or autoionization. Such autoionization peaks dominate the electron spectrum obtained in independent measurements. We expect that atomic lines will prevail in the fluorescence spectrum as well. Further calculations would be needed to elucidate the full decay dynamics where electronic decay and molecular dissociation compete on the same time scale. With the development of free-electron lasers, using an x-ray pulse as a pump and an infrared laser as a probe might allow one in the future to investigate the Auger decay, molecular dissociation, and autoionization of O$_2$ in real time.

[1] J. Adachi, N. Kosugi, and A. Yagishita, J. Phys. B **38**, R127 (2005).

[2] H. Ågren, L. Yang, V. Carravetta, and L. G. M. Pettersson, Chem. Phys. Lett. **259**, 21 (1996).

[3] A. Kivimaki, B. Kempgens, M. N. Piancastelli, M. Neeb, K. Maier, A. Rudel, U. Hergenhahn, and A. M. Bradshaw, J. Electron Spectrosc. Relat. Phenom. **93**, 81 (1998).

[4] N. Kosugi, E. Shigemasa, and A. Yagishita, Chem. Phys. Lett. **190**, 481 (1992).

[5] Y. Ma, C. T. Chen, G. Meigs, K. Randall, and F. Sette, Phys. Rev. A **44**, 1848 (1991).

[6] M. Neeb, J. E. Rubensson, M. Biermann, and W. Eberhardt, Phys. Rev. Lett. **71**, 3091 (1993).

[7] A. Yagishita, E. Shigemasa, and N. Kosugi, Phys. Rev. Lett. **72**, 3961 (1994).

[8] M. Coreno, M. de Simone, K. C. Prince, R. Richter, M. Vondracek, L. Avaldi, and R. Camilloni, Chem. Phys. Lett. **306**, 269 (1999).

[9] S. L. Sorensen, K. J. Borve, R. Feifel, A. de Fanis, and K. Ueda, J. Phys. B **41**, 095101 (2008).

[10] J. D. Bozek, S. E. Canton, E. Kukk, and N. Berrah, Chem. Phys. **289**, 149 (2003).

[11] M. N. Piancastelli, J. Electron Spectrosc. Relat. Phenom. **107**, 1 (2000).

[12] S. L. Sorenson and S. Svensson, J. Electron Spectrosc. Relat. Phenom. **114-116**, 1 (2001).

[13] K. Ueda, J. Phys. B **36**, R1 (2003).

[14] K. Ueda, J. Phys. Soc. Jpn. **75**, 032001 (2006).

[15] T. Tanaka, R. Feifel, M. Kitajima, H. Tanaka, S. L. Sorensen, R. Sankari, A. De Fanis, M. N. Piancastelli, L. Karlsson, and K. Ueda, Phys. Rev. A **78**, 022516 (2008).

[16] O. Björneholm, M. Bassler, A. Ausmees, I. Hjelte, R. Feifel, H. Wang, C. Miron, M. N. Piancastelli, S. Svensson, S. L. Sorensen, F. Gel'mukhanov, and H. Ågren, Phys. Rev. Lett. **84**, 2826 (2000).

[17] X.-J. Liu, Q. Miao, F. Gel'mukhanov, M. Patanen, O. Travnikova, C. Nicolas, H. Ågren, K. Ueda, and C. Miron, Nat. Photon. **9**, 120 (2014).

[18] H. Sann, T. Havermeier, C. Müller, H. K. Kim, F. Trinter, M. Waitz, J. Voigtsberger, F. Sturm, T. Bauer, R. Wallauer, D. Schneider, M. Weller, C. Goihl, J. Tross, K. Cole, J. Wu, M. S. Schöffler, H. Schmidt-Böcking, T. Jahnke, M. Simon, and R. Dörner, Phys. Rev. Lett. **117**, 243002 (2016).

[19] P. Morin and C. Miron, J. Electron Spectrosc. Relat. Phenom. **185**, 259 (2012).

[20] M. Lundqvist, D. Edvardsson, P. Baltzer, M. Larsson, and B. Wannberg, J. Phys. B **29**, 499 (1996).

[21] Y. Hikosaka, T. Aoto, R. I. Hall, K. Ito, R. Hirayama, N. Yamamoto, and E. Miyoshi, J. Chem. Phys. **119**, 7693 (2003).

[22] J. H. D. Eland, O. Vieuxmaire, T. Kinugawa, P. Lablanquie, R. I. Hall, and F. Penent, Phys. Rev. Lett. **90**, 053003 (2003).

[23] R. Feifel, J. H. D. Eland, and D. Edvardsson, J. Chem. Phys. **122**, 144308 (2005).

[24] G. Prümper, V. Carravetta, Y. Muramatsu, Y. Tamenori, M. Kitajima, H. Tanaka, C. Makochekanwa, M. Hoshino, X. J. Liu, and K. Ueda, Phys. Rev. A **76**, 052705 (2007).

[25] O. Kugeler, G. Prümper, R. Hentges, J. Viefhaus, D. Rolles, U. Becker, S. Marburger, and U. Hergenhahn, Phys. Rev. Lett. **93**, 033002 (2004).

[26] R. Dörner, T. Weber, M. Weckenbrock, A. Staudte, M. Hattass, H. Schmidt-Böcking, R. Moshammer, and J. Ullrich, Adv. At., Mol., Opt. Phy. **48**, 1 (2002).

[27] J. Ullrich, R. Moshammer, A. Dorn, R. Dörner, L. P. H. Schmidt, and H. Schmidt-Böcking, Rep. Prog. Phys. **66**, 1463 (2003).

[28] A. S. Sandhu, E. Gagnon, R. Santra, V. Sharma, W. Li, P. Ho, P. Ranitovic, C. L. Cocke, M. M. Murnane, and H. C. Kapteyn, Science **322**, 1081 (2008).

[29] T. Jahnke, T. Weber, T. Osipov, A. Landers, O. Jagutzki, L. Schmidt, C. Cocke, M. Prior, H. Schmidt-Böcking, and R. Dörner, J. Electron Spectrosc. Relat. Phenom. **141**, 229 (2004).

[30] P. Morin, M. Simon, C. Miron, N. Leclercq, and D. Hansen, J. Electron Spectrosc. Relat. Phenom. **93**, 49 (1998).

[31] C. Miron and P. Morin, Nucl. Instrum. Methods Phys. Res., A **601**, 66 (2009).

[32] C. Miron, M. Simon, N. Leclercq, and P. Morin, Rev. Sci. Instrum. **68**, 3728 (1997).

[33] K. Le Guen, D. Céolin, R. Guillemin, C. Miron, N. Leclercq, M. Bougeard, M. Simon, P. Morin, A. Mocellin, F. Burmeister, A. Naves de Brito, and S. L. Sorensen, Rev. Sci. Instrum. **73**, 3885 (2002).

[34] X.-J. Liu, C. Nicolas, and C. Miron, Rev. Sci. Instrum. **84**, 033105 (2013).

[35] RoentDek Handels GmbH, www.Roentdek.com.

[36] G. Prümper and K. Ueda, Nucl. Instrum. Methods Phys. Res., A **574**, 350 (2007).

[37] R. I. Hall, G. Dawber, A. McConkey, M. A. MacDonald, and G. C. King, Phys. Rev. Lett. **68**, 2751 (1992).

[38] X. J. Liu, C. Nicolas, M. Patanen, and C. Miron, Sci. Rep. **7**, 2898 (2017).

[39] D. Edvardsson, S. Lunell, F. Rakowitz, C. M. Marian, and L. Karlsson, Chem. Phys. **229**, 203 (1998).

[40] Atomic Spectra Database, physics.nist.gov/asd/ (2016).

[41] P. M. Dehmer, W. L. Luken, and W. A. Chupka, J. Chem. Phys. **67**, 195 (1977).

[42] T. Gejo, M. Oura, T. Tokushima, Y. Horikawa, H. Arai, S. Shin, V. Kimberg, and N. Kosugi, J. Chem. Phys. **147**, 044310 (2017).

[43] K. Ueda (personal communication).